Pseudo non-diffracting beam array through high-indexed dielectric metaplate

Pseudo non-diffracting beam array through high-indexed dielectric metaplate

Isma Javed[1], Muhammad Ashar Naveed[1], Muhammad Zubair[1], Kashif Riaz[1], Muhammad Qasim Mehmood[1], Yehia Massoud[2,*]

[1]MicroNano Lab, Electrical Engineering Department, Information Technology University (ITU) of the Punjab, Ferozepur Road, Lahore 54600, Pakistan.

[2]Innovative Technologies Laboratories (ITL), King Abdullah University of Science and Technology (KAUST), Thuwal 23955, Saudi Arabia.

*yehia.massoud@kaust.edu.sa

***Abstract*— Highly non-diffracting bessel beams have gathered an excessive amount of significance due to their several applications ranging from optical communication, displays to trapping and manipulation. Array of bessel beams with multiple orders is generated by utilizing geometric metasurfaces to have full phase control over optical properties of light. In prior works, Bessel beams are realized with optical metasurfaces of titanium dioxide (TiO_2) and gallium nitride (GaN) but they have bottlenecks in terms of complex and expensive fabrication. Here, in this manuscript we have represented single layer optical metasurface based on gallium phosphide (GaP) for Bessel beam generation. The proposed metasurface has high transmission efficiency in visible regime and capable of producing four bessel beams of arbitrary orders without the accumulation of extra complexities in conventional nano-rectangular pillar geometry. Due to property of orbital angular momentum, these arbitrary order bessel beams have high capacity for data storage. Thus, they provide an appropriate plateform for numerous interesting phenomena of data encryption and information storage.**

Keywords—Optical metasurfaces; Gallium phosphide; Bessel beam; PB-phase.

I. INTRODUCTION

Bessel beams have procured ample amount of researchers concentration due to their distinctive properties of self-reconstruction and non-diffraction and offered optical pulling forces [1]. Because of these unique properties, bessel beams have founded numerous applications like microscopy, optical communication, trapping, manipulation, etc. [2, 3]. Bessel beams were firstly discovered by Durnin et al. in 1987 as the non-diffracting set of solutions of the free space Helmholts equation [8]. The optical response of bessel beams described by their transverse electric field profile $\mathcal{E}(r,\varphi,z)$ propagating in z direction can be defined as:

$$\mathcal{E}(r,\varphi,z) = \left(E.e^{i(k_z z \pm n\varphi)}\right).J_n(k_r r) \qquad (1)$$

where E depicts amplitude, the $J_n(k_r r)$ is the bessel function of 1st kind, k_r and k_z are wavevectors in transverse and longitudinal direction satisfying the equation $\sqrt{k_r^2 + k_z^2} = \frac{2\pi}{\lambda}$. Equation 1 demonstrates that the electric field profile of bessel beams as a function of phase φ. It can be characterized by bessel function of first kind. Equation 1 also depicts that the transverse electric field profile is independent of propagation direction, making them non-diffracting and havings zero intensity for $n \neq 0$ due to phase singularities. The spatial phase term $e^{\pm in\varphi}$ in electric field provides characteristics of orbital angular momentum (OAM) to bessel beam [4].

During the past few years, control over the phase discontinuities along the interface between to mediums has been achieved by flat surfaces known as metasurfaces, composed of sub-wavelength resonators arranged in a periodic/aperiodic manner. Suitable selection of material, geometry, and orientation of sub-wavelength resonators allow metasurfaces to cover full phase range of 0 to 2π, which have paved the path to various interesting applications such as holography [5, 6], color printing [7, 8], wave-absorption [9, 10], bessel beams generation [11], and polarization conversion [12, 13].

In prior work, many transmission-type metallic metasurfaces were reported [14], which have significant drawbacks such as anomalous reaction due to light scattering and low efficiencies due to ohmics losses associated with metals. Also, the bessel beams generated from plasmonic metasurfaces have low numerical aperture. To avoid such short-comings, reflection type metasurfaces have been proposed [15], but still, this approach has a bottleneck in imaging techniques. However, Si-based metasurfaces have provided promising results in the infrared regime but have suffered high absorption in the visible regime [16]. To overcome this constraint, all-dielectric type metasurfaces based on TiO_2 and GaN have high transmission efficiency and low absorption coefficient reported in Ref. [17] and [18], respectively. However, such flat surfaces have very expensive and complex fabrications and also have high aspect ratio issues.

Here, we have demonstrated all-dielectric transmission type metasurface-based bessel beam generation using GaP. The metasurface has high transmission efficiency and negligible absorption in broadband and almost cover whole visible regime of EM spectrum. Moreover, the metasurface can generate a number of bessel beams with different orders under the incidence of left circular polarized (LCP) light, as shown in Fig. 1. The preliminary work of this is represented in [19].

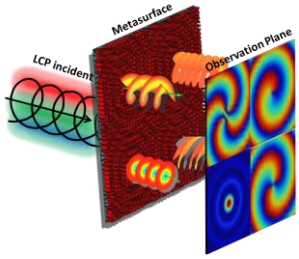

Fig. 1: Conceptual diagram of the proposed metasurface. Array of four Bessel beams with 0th, 1st, 2nd and 4th order are generated in +z-direction under the incidence of LCP light coming from the –z-direction.

II. Design Methodology

The nano-rectangular pillars are selected as meta-atom which is the basic building block of the metasurface. The meta-atom consists of the gallium phosphide (GaP) based nano-pillar with length *L*, width *W* and height *H* and is placed upon the silicon dioxide (SiO_2) substrate of period *P* as shown in Fig 2b. The ellipsometric data of optical constants for GaP is shown in Fig 2a. It is noticeable that it provides a large transparent window with high refractive index which makes it potential candidate for optical metasurface design.

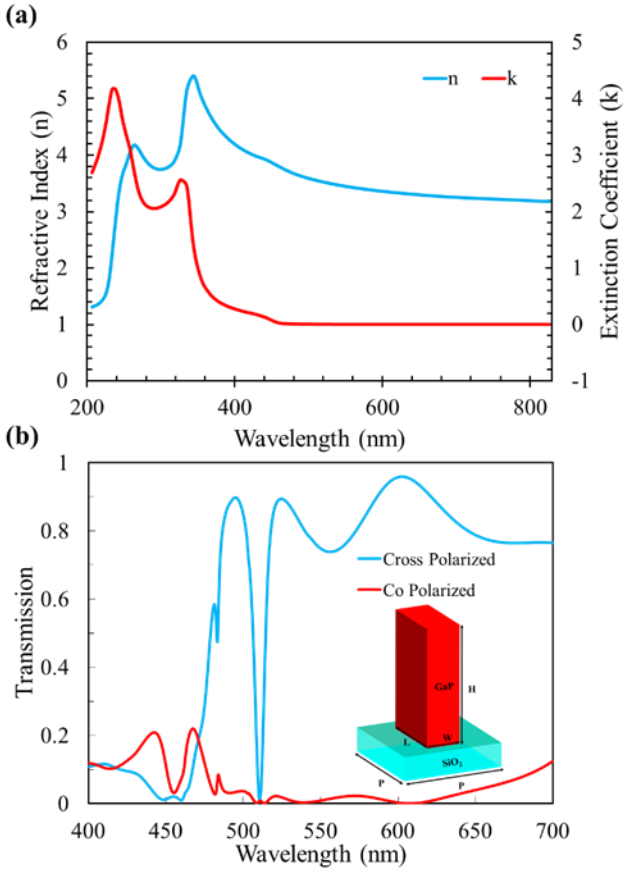

Fig. 2: a) Optical constants of GaP. b) Geometry of unit cell with its transmission efficiencies. Schematic of unit cell (represented inside the plot) consists on GaP over the SiO_2 substrate. Physical dimensions of unit cell are *L*=210nm, *W*=90nm, *H*=380nm and *P*=250nm. Cross and co-polarization transmission efficiencies of unit cell are also depicted. It gives maximum cross polarized transmission (>80%) and minimum co-polarized transmission (<10%) in visible regime (480nm-700nm.

The designed nano-rectangular pillar acts as a half waveplate i.e., convert the LCP light into right circular polarized (RCP) light and vice versa in order to maximize the performance. To attain the desired phase, a full phase range of 0 to 2π is achieved by exploiting the Pancharatnam–Berry (PB) phase associated with the in-plane angular orientation of nano-rectangular pillars. In order to maximize the cross-polarization efficiency, the *L*, *W*, and *H* are optimized using finite difference time domain (FDTD) and apply perfectly matched layer (PML) in the z-direction and periodic boundary conditions in remaining directions. As a result, cross-polarization efficiency is greater than 80% has been achieved for the wavelength band of 480nm to 700nm except for a narrow band of 505nm to 530nm where efficiency is degraded while co-polarization efficiency remains less than 10% in the entire band (480nm-700nm). In order to attain the bessel beams of a different order, the required phase profile $\varphi_r(x, y)$ can be described by:

$$\varphi_r(x,y) = 2\pi - \frac{2\pi}{\lambda_0}\sqrt{x^2+y^2}.NA + l.tan^{-1}(^{y}/_{x}) \quad (2)$$

Where NA is the numerical aperture, λ_0 is the operating wavelength, , x and y are positioned in a plane while l is the topological charge. By changing the l , a number of intertwined phase fronts change in the imaging plane gives rise to different order bessel beams. The designed metasurface generates four bessel beams of distinct orders by changing the l from 0 to 4.

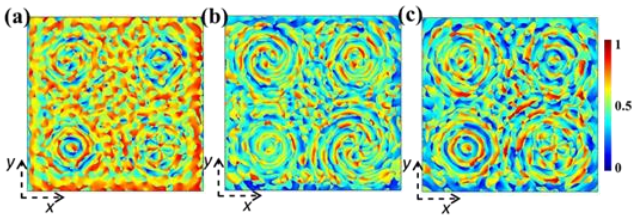

Fig. 3: Simulated results of phase distribution of designed metasurface (a) at wavelength λ_o = 488nm (a) at wavelength λ_o = 532nm and (c) at wavelength λ_o = 633nm.

III. Results And Discussion

After achieving full control over the phase, four bessel beams with 0^{th}, 1^{st}, 2^{nd}, and 4^{th} order respectively are realized using commercial software CST Microwave Studio. Fig. 4 shows the simulated electric field distribution in different plane configurations. Fig. 4a1 shows the electric field profile of all four bessel beams of distinct orders at λ_o= 488nm. In the top half-plane of electric field profile, 1^{st} and 2^{nd} order bessel beams are generated, while in the bottom half-plane, 4^{th} and 0^{th} order bessel beams are generated from right to left, respectively. Similarly, Fig. 4b1 and Fig. 4c1 shows the electric field intensity at λ_o = 532nm and λ_o = 633nm respectively. Similarly (b1, b2, b3) simulated electric field intensity at wavelength λ_o = 532nm and (c1, c2, c3) at wavelength λ_o = 633nm respectively. The transverse electric field distribution of 0^{th} and 2^{nd} order bessel beams in

propagating direction at wavelengths of λ_o= 488nm , λ_o= 532nm and λ_o= 633nm are demonstrated in Fig. 4a2, Fig. 4b2 and Fig. 4c2 respectively. While propagating direction electric field intensity of 1st and 4th order bessel beams at all three wavelengths are shown in Fig. 4(a3-c3). For all three wavelengths, metasurface shows promising results. Interweaved phase profile are formed for higher-order bessel beams at three different optical wavelengths, as shown in Fig. 3, which give rise to OAM.

IV. CONCLUSION

In summary of the work, we have realized the multiple order bessel beam generation using the efficient optical all dielectric metasurface in transmission mode. For this purpose gallium phosphide based nano- rectangular pillar has been optimized such that it acts as half waveplate in visible domain. For full phase coverage and manipulation, PB-phase is utilized. The zero, first, second and fourth order bessel beams are shown at three different wavelengths i.e. 488nm, 532nm and 633nm which retain orbital angular momentum. Arbitrary multi-order Bessel beams with high transmission and negligible loses in optical regime makes the metasurface a highly recommended choice for various applications like data encryption and manipulation, data transportation, optical communication, trapping and displays.

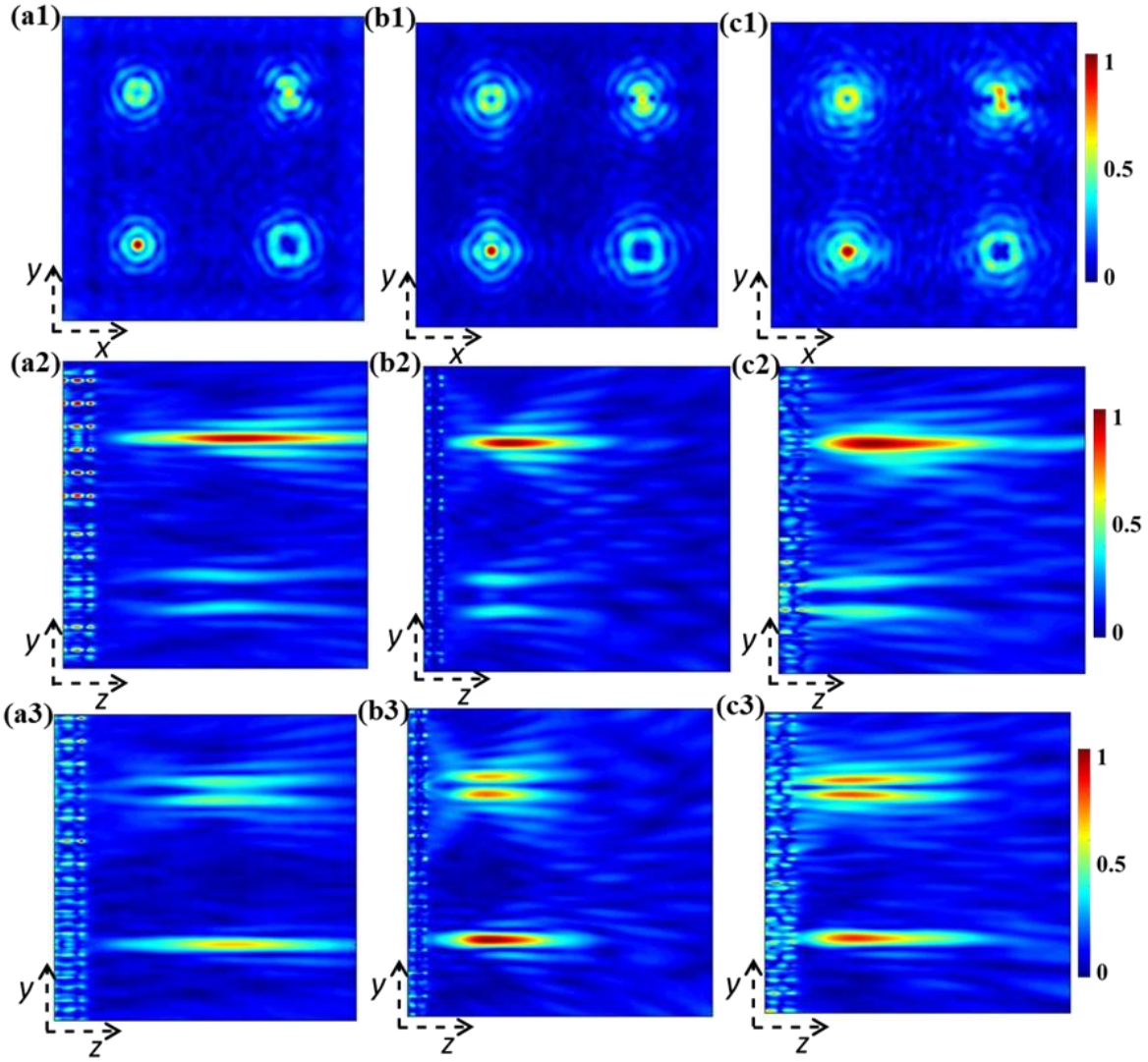

Fig 4: Optical characterization of bessel beams of different orders with NA=0.7. (a1, a2, a3) Simulated electric field intensity at wavelength λ0 = 488nm in xy-plane, yz-plane at x=-2500nmm and yz-plane at x=2500nmm respectively. Similarly (b1, b2, b3) simulated electric field intensity at wavelength λ0 = 532nm and (c1, c2, c3) at wavelength λ0 = 633nm respectively.

REFERENCES

[1] Z. Bouchal, J. Wagner, and M. Chlup, "Self-reconstruction of a distorted nondiffracting beam," *Optics communications*, vol. 151, no. 4-6, pp. 207-211, 1998.

[2] F. O. Fahrbach, P. Simon, and A. Rohrbach, "Microscopy with self-reconstructing beams," *Nature photonics*, vol. 4, no. 11, pp. 780-785, 2010.

[3] V. Garcés-Chávez, D. McGloin, H. Melville, W. Sibbett, and K. Dholakia, "Simultaneous micromanipulation in multiple planes using a self-reconstructing light beam," *Nature*, vol. 419, no. 6903, pp. 145-147, 2002.

[4] J. Courtial, K. Dholakia, L. Allen, and M. Padgett, "Gaussian beams with very high orbital angular momentum," *Optics communications*, vol. 144, no. 4-6, pp. 210-213, 1997.

[5] M. A. Naveed *et al.*, "A Pragmatic Metasurface with Asymmetric Spin Interactions," in *CLEO: QELS_Fundamental Science*, 2020: Optical Society of America, p. FM4B. 5.

[6] M. A. Ansari *et al.*, "A spin-encoded all-dielectric metahologram for visible light," *Laser & Photonics Reviews*, vol. 13, no. 5, p. 1900065, 2019.

[7] T. Lee, J. Jang, H. Jeong, and J. Rho, "Plasmonic-and dielectric-based structural coloring: from fundamentals to practical applications," *Nano Convergence*, vol. 5, no. 1, pp. 1-21, 2018.

[8] X. Liu, Z. Huang, and J. Zang, "All-dielectric silicon nanoring metasurface for full-color printing," *Nano Letters*, vol. 20, no. 12, pp. 8739-8744, 2020.

[9] R. Bilal, M. Naveed, M. Baqir, M. Ali, and A. Rahim, "Design of a wideband terahertz metamaterial absorber based on Pythagorean-tree fractal geometry," *Optical Materials Express*, vol. 10, no. 12, pp. 3007-3020, 2020.

[10] M. A. Naveed, R. M. H. Bilal, M. A. Baqir, M. M. Bashir, M. M. Ali, and A. A. Rahim, "Ultrawideband fractal metamaterial absorber made of nickel operating in the UV to IR spectrum," *Optics Express*, vol. 29, no. 26, pp. 42911-42923, 2021.

[11] Z. Li *et al.*, "Dielectric meta-holograms enabled with dual magnetic resonances in visible light," *ACS nano*, vol. 11, no. 9, pp. 9382-9389, 2017.

[12] T. Ahmad *et al.*, "Ultrawideband Cross-Polarization Converter Using Anisotropic Reflective Metasurface," *Electronics*, vol. 11, no. 3, p. 487, 2022.

[13] G. Dong, H. Shi, S. Xia, A. Zhang, Z. Xu, and X. Wei, "Ultra-broadband perfect cross polarization conversion metasurface," *Optics Communications*, vol. 365, pp. 108-112, 2016.

[14] F. Aieta *et al.*, "Aberration-free ultrathin flat lenses and axicons at telecom wavelengths based on plasmonic metasurfaces," *Nano letters*, vol. 12, no. 9, pp. 4932-4936, 2012.

[15] G. Zheng, H. Mühlenbernd, M. Kenney, G. Li, T. Zentgraf, and S. Zhang, "Metasurface holograms reaching 80% efficiency," *Nature nanotechnology*, vol. 10, no. 4, pp. 308-312, 2015.

[16] M. A. Naveed *et al.*, "Optical spin-symmetry breaking for high-efficiency directional helicity-multiplexed metaholograms," *Microsystems & Nanoengineering*, vol. 7, no. 1, pp. 1-9, 2021.

[17] W. T. Chen *et al.*, "Generation of wavelength-independent subwavelength Bessel beams using metasurfaces," *Light: Science & Applications*, vol. 6, no. 5, pp. e16259-e16259, 2017.

[18] B. H. Chen *et al.*, "GaN metalens for pixel-level full-color routing at visible light," *Nano letters*, vol. 17, no. 10, pp. 6345-6352, 2017.

[19] https://www.ursi.org/proceedings/procGA21/papers/ URSIGASS 2021-Tu-FIP-DBI-11.pdf